

Variational Bayes for Robust Radar Single Object Tracking

Alp Sari
TU Eindhoven
Eindhoven, Netherlands
a.sari@student.tue.nl

Tak Kaneko
Sioux Technologies
Eindhoven, Netherlands

Lense H.M. Swaenen
Sioux Technologies
Eindhoven, Netherlands

Wouter M. Kouw
TU Eindhoven
Eindhoven, Netherlands
w.m.kouw@tue.nl

Abstract—We address object tracking by radar and the robustness of the current state-of-the-art methods to process outliers. The standard tracking algorithms extract detections from radar image space to use it in the filtering stage. Filtering is performed by a Kalman filter, which assumes Gaussian distributed noise. However, this assumption does not account for large modeling errors and results in poor tracking performance during abrupt motions. We take the Gaussian Sum Filter (single-object variant of the Multi Hypothesis Tracker) as our baseline and propose a modification by modelling process noise with a distribution that has heavier tails than a Gaussian. Variational Bayes provides a fast, computationally cheap inference algorithm. Our simulations show that - in the presence of process outliers - the robust tracker outperforms the Gaussian Sum filter when tracking single objects.

Index Terms—Gaussian Sum Filter, Object Tracking, Radar, Robustness, t-distribution, Variational Bayes.

I. INTRODUCTION

Radar systems detect objects by emitting electromagnetic waves in the radio spectrum and capturing the signal reflected off objects. They are a critical part of Autonomous Driving (AD) systems for their robustness in varying weather and lighting conditions [1]. Traditional radar tracking algorithms have a processing chain: the detection stage extracts signal intensity peaks from raw measurements, the clustering stage replaces groups of peaks with points, the data association stage assigns these points to objects of interest (e.g., vehicles, pedestrians) and the filtering stage refines the state estimates of the objects [2]. We propose an alteration to the filtering stage to increase the robustness to modelling error.

Single object tracking algorithms include the Nearest Neighbour filter, the Probabilistic Data Association filter and the Gaussian Sum Filter [3]. Unlike Nearest Neighbour and Probabilistic Data Association, the Gaussian Sum Filter considers multiple hypotheses, which improves performance at the cost of increased computational complexity. All of these use a Kalman filter during the filtering stage, which is the optimal estimator in the presence of additive Gaussian process and measurement noise [4] [5]. Unfortunately, it is not optimal in the presence of non-Gaussian noise. For example, consider an automotive radar setting that assumes that other cars behave according to constant velocity or constant acceleration dynamics. Sudden movements, such as emergency brakes, generate

state evolutions that lie far out in the tails of the Gaussian noise distribution. The probabilities of these points are underestimated which affects the subsequent steps in reasoning over multiple hypotheses, ultimately degrading performance. These outliers are modelling errors, arising from the difference between the system’s behavior and the model’s assumptions. This paper proposes an alternate noise model, namely the heavy-tailed Student’s t-distribution, to avoid underestimation of outlying state dynamics. Specifically, we replace the Kalman filter block of Gaussian Sum Filter with the Robust Student’s t Kalman filter [6], which increases the overall algorithm’s robustness to model errors.

Our key contributions are: a demonstration of the GSF’s susceptibility to noise model error, a model specification and inference algorithm using a Student’s t-distribution noise model, and a performance comparison between the proposed algorithm and the GSF. Simulated experiments show that the resulting filter is more robust to noise model errors.

II. PROBLEM SETTING

Consider an object with state $x_k \in \mathbb{R}^{D_x}$ that generates a measurement $o_k \in \mathbb{R}^{D_o}$, corresponding to a peak in signal power. The detection stage finds the peak - along with peaks produced by noise - and outputs a series of point detections $Z_k = \{z_k^i \in \mathbb{R}^{D_o} : i = 1, \dots, m_k\}$. Note that it is also possible that the object was not detected by the peak-finder, in which case all Z_k correspond to noise peaks, a.k.a. *clutter*. Our goal is to recursively infer the state distribution given all detections so far, i.e., estimate $p(x_k | Z_{1:k})$ [7].

To indicate which detection corresponds to the object measurement, we introduce a data association variable $\theta_k \in \{0, 1, \dots, m_k\}$ such that $z_k^{\theta_k} = o_k$. Our likelihood then becomes a joint probability over data associations and detections, i.e., $p(\theta_k, Z_k | x_k)$. Using the Bayesian filtering equations [7, Ch. 4], we may write:

$$p(x_k | \theta_{1:k}, Z_{1:k}) = \frac{p(\theta_k, Z_k | x_k) p(x_k | \theta_{1:k-1}, Z_{1:k-1})}{p(\theta_k, Z_k | \theta_{1:k-1}, Z_{1:k-1})}, \quad (1)$$

where the numerator consists of the likelihood times the prior predictive distribution and the denominator is the evidence term. The special case $\theta_k = 0$ indicates that none of the

detections correspond to the object. In that case, the observations are not dependent on the object, $p(\theta_k = 0, Z_k | x_k) = p(\theta_k = 0, Z_k)$, and the state posterior in Equation (1) will be proportional to the prior predictive, a situation equivalent to filtering with "missing" observations.

Note that Equation (1) is an intermediate posterior distribution as it still depends on the data associations. To obtain the exact state posterior, we must marginalize over $\theta_{1:k}$. This marginalization corresponds to weighting each possible data association, i.e., each possible sequence of object evolutions, with their probability:

$$p(x_k | Z_{1:k}) = \sum_{\theta_1} \dots \sum_{\theta_k} p(x_k | \theta_{1:k}, Z_{1:k}) \Pr[\theta_{1:k} | Z_{1:k}] \quad (2)$$

where $\Pr[\cdot]$ refers to a probability mass function. But here we find a problem: the number of hypothetical sequences is $\prod_{j=1}^k (m_j + 1)$. Calculating the exact posterior quickly becomes intractable, which indicates a need for approximation.

A. Gaussian Sum Filter

The Gaussian Sum Filter (GSF) approximates the posterior distribution by a Gaussian mixture model with fewer components than the original mixture. The GSF models the state transition $p(x_k | x_{k-1})$ and measurement model of a single detection $p(z_k^{\theta_k} | x_k)$ by a linear state space model with additive Gaussian noise. Clutter detections are modeled with a Poisson Point Process (Poisson Random Finite Set) with an intensity function $\lambda_c(\cdot)$ [8]. Then, the conditional posterior distribution $p(x_k | \theta_k, Z_k)$ is calculated using the Kalman filter (KF) equations. Also, the calculation of the mixture weights $\Pr[\theta_k | Z_k]$ requires the evidence term $p(z_k^{\theta_k})$, which has a tractable expression, given model specifications above.

After obtaining the conditional posteriors and weights, the GSF performs a mixture reduction step, which is a complex problem in itself. We choose the following simple approach: We cap the maximum number of components at N_{\max} and prune the components with weights smaller than a threshold γ_{prune} . If we are left with more than N_{\max} components, Runnall's algorithm [9] is used to reduce to mixture to N_{\max} components.

B. Susceptibility to Process Outliers

The GSF has a zero mean Gaussian noise model for the process noise, which accounts for the mismatch between the modeled dynamics of the target and the true motion dynamics. Note that the Gaussian distribution has slim tails, and 99.7% of the probability mass falls into the ± 3 standard deviation around the mean value. Thus, the mismatch between the model and true dynamics is explained well by the Gaussian noise if the error is in ± 3 standard deviation. But, when the target moves differently than the expected motion dynamics, the error increases and the error values fall into the tails of the Gaussian, which are referred as outliers. When an outlier is encountered, the Gaussian distributed process noise underestimates its probability density. An illustration of the

problem is shown in Fig. 1. We simulate the observation of positions in clutter. The observed detections are shown with black dots in the position plots (top). The blue dashed line is the state estimate using GSF and the corresponding ribbon indicates the ± 3 standard deviation of the state estimate. At the 20th time step (indicated by a vertical red dashed line), the state transition is corrupted with an outlier value and it is observed that the state estimation drifts off.

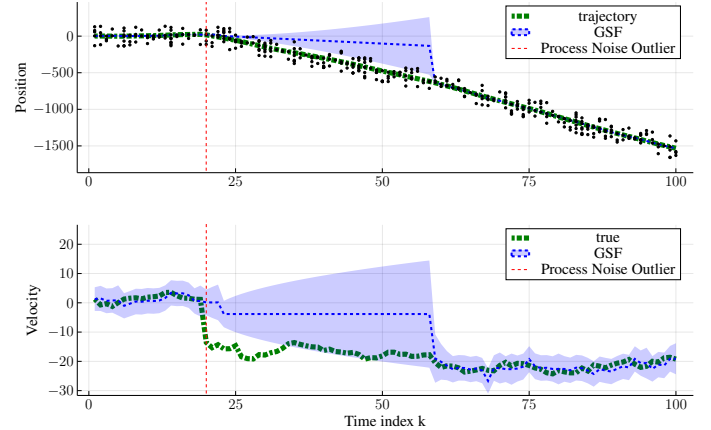


Fig. 1: A simulated tracking scenario. Position (top), velocity (bottom) and corresponding confidence interval estimates over time of GSF (blue-dashed) versus true trajectory (green-dashed). Black dots refer to detections (including clutter). The vertical line (red) indicates when the process outlier is introduced.

III. ROBUST EXTENSION OF GSF

We will model both the measurement and the predictive prior distribution with a Student's t-distribution to address the susceptibility to process outliers (Sec. II-B). The Student's t-distribution has heavier tails than the Gaussian distribution, but inference using the Student's t is intractable. We perform approximate inference using variational Bayes (VB). The resulting filtering algorithm is known as the Robust Student's t Kalman filter (RSTKF). The RSTKF and VB update equations have previously been derived in [6], and this paper is an extension towards single object tracking using the GSF algorithm.

A. Model Specification

Consider a discrete-time linear state-space model with additive noise expressed as:

$$x_k = Fx_{k-1} + \omega_k \quad (3a)$$

$$o_k = Hx_k + \nu_k, \quad (3b)$$

where F is the state transition matrix, H is the observation matrix, and ω_k and ν_k are referred as process and measurement noise, respectively. In probabilistic form, this becomes:

$$p(x_k | x_{k-1}) = p_{\omega_k}(x_k - Fx_{k-1}) \quad (4a)$$

$$p(o_k | x_k) = p_{\nu_k}(o_k - Hx_k), \quad (4b)$$

where $p_{\omega_k}(\cdot)$ and $p_{\nu_k}(\cdot)$ are the process noise and measurement noise pdfs, respectively. Using (3a), the predictive prior is obtained through the Chapman-Kolmogorov equation which in this case yields [7, Ch. 3]:

$$\begin{aligned} p(x_k | o_{1:k-1}) &= \int p_{\omega_k}(x_k - Fx_{k-1}) p(x_{k-1} | o_{1:k-1}) dx_{k-1}. \end{aligned} \quad (5)$$

A standard KF assumes Gaussian noise distributions, with zero mean vectors and covariance matrices Q and R , respectively. Then, the predictive prior and likelihood terms are computed as:

$$p(x_k | o_{1:k-1}) = \mathcal{N}(x_k | \mu_k |_{k-1}, P_k |_{k-1}) \quad (6a)$$

$$p(o_k | x_k) = \mathcal{N}(o_k | Hx_k, R), \quad (6b)$$

where $\mu_k |_{k-1}$ and $P_k |_{k-1}$ are:

$$\mu_k |_{k-1} = F\mu_{k-1} |_{k-1}, \quad P_k |_{k-1} = FP_{k-1} |_{k-1}F^T + Q. \quad (7)$$

Instead of a Gaussian, we adopt a Student's t-distribution for the predictive prior and likelihood, which gives:

$$p(x_k | o_{1:k-1}, \Sigma_k) = \mathcal{T}(x_k | \mu_k |_{k-1}, \Sigma_k, s) \quad (8a)$$

$$p(o_k | x_k) = \mathcal{T}(o_k | Hx_k, R, v), \quad (8b)$$

where $\mathcal{T}(x | \mu, \Lambda, s)$ denotes a generalized Student's t-distribution with location μ , scale matrix Λ and degrees of freedom s . We treat scale matrix of the prior term Σ_k as an unknown random variable, which increases the uncertainty factored into the model.

Aside from being a distribution with a heavier tail, the Student's t-distribution can also be expressed as an infinite mixture of Gaussians with the same mean but different scales:

$$\begin{aligned} \mathcal{T}(x_k | \mu_k |_{k-1}, \Sigma_k, s) &= \int \mathcal{N}\left(x_k | \mu_k |_{k-1}, \frac{\Sigma_k}{\xi_k}\right) \mathcal{G}\left(\xi_k | \frac{s}{2}, \frac{s}{2}\right) d\xi_k \end{aligned} \quad (9a)$$

$$\begin{aligned} \mathcal{T}(o_k | Hx_k, R, v) &= \int \mathcal{N}\left(o_k | Hx_k, \frac{R}{\lambda_k}\right) \mathcal{G}\left(\lambda_k | \frac{v}{2}, \frac{v}{2}\right) d\lambda_k, \end{aligned} \quad (9b)$$

where $\mathcal{G}(\cdot | \alpha, \beta)$ denotes a Gamma distribution with shape parameter α and rate parameter β , ξ_k and λ_k are scale parameters. Infinite mixture representation shows that model specification in (8) is richer than (6), which only has a single Gaussian expression. Moreover, the model specification can be written as a hierarchical state space model using (9a) and (9b). The predictive prior of the hierarchical state space model is:

$$p(x_k | \Sigma_k, \xi_k, o_{1:k-1}) = \mathcal{N}(x_k | \mu_k, \Sigma_k / \xi_k) \quad (10a)$$

$$p(\Sigma_k) = \mathcal{IW}(\Sigma_k | u_k, U_k) \quad (10b)$$

$$p(\xi_k) = \mathcal{G}\left(\xi_k | \frac{s}{2}, \frac{s}{2}\right), \quad (10c)$$

where $\mathcal{IW}(\Sigma_k | u_k, U_k)$ denotes the inverse-Wishart distribution with u_k degrees of freedom and scale matrix U_k . The

scale matrix is set as $U_k = P_k |_{k-1} \cdot (u_k - D_x - 1)$ to ensure $\mathbb{E}[\Sigma_k] = P_k |_{k-1}$. The likelihood hierarchical model is:

$$p(o_k | \lambda_k, x_k) = \mathcal{N}(o_k | Hx_k, R_k / \lambda_k) \quad (11a)$$

$$p(\lambda_k) = \mathcal{G}\left(\lambda_k | \frac{v}{2}, \frac{v}{2}\right). \quad (11b)$$

Note that the model specification in (10) and (11) is a special case of Gaussian Scale Mixture (GSM) distribution. More flexibility, such as skewed heavy-tailed distributions, can be introduced using this framework. For more details about GSM distributions, we refer the interested reader to [10].

Unfortunately, with the given model specification, computing the posterior $p(x_k, \Sigma_k, \xi_k, \lambda_k | o_{1:k})$ exactly is intractable.

B. Inference using Variational Bayes

Variational Bayes refers to adopting a second probabilistic model, called the *variational* model q , and approximating the original model using the calculus of variations [11]. The variational model is optimized through the *free energy* functional at time step k :

$$\mathcal{F}_k[q] \triangleq \mathbb{E}_q \left[\ln \frac{q(x_k, \Sigma_k, \xi_k, \lambda_k)}{p(x_k, \Sigma_k, \xi_k, \lambda_k | o_{1:k})} \right] - \ln p(o_k | o_{1:k-1}). \quad (12)$$

The first term is a Kullback-Leibler (KL) divergence between the variational model and the posterior distribution, indicating the quality of the approximation. However, evaluating this expression requires the true posterior distribution. This problem can be circumvented by applying Bayes' rule:

$$\begin{aligned} \mathcal{F}_k[q] &= \mathbb{E}_q \left[\ln \frac{q(x_k, \Sigma_k, \xi_k, \lambda_k)}{p(x_k, \Sigma_k, \xi_k | o_{1:k-1})} \right] \\ &\quad - \mathbb{E}_q \left[\ln p(o_k, \lambda_k | x_k) \right], \end{aligned} \quad (13)$$

where the posterior times the evidence was decomposed into the prior, corresponding to (10), and the likelihood, corresponding to (11).

The minimisation of the free energy functional requires the calculus of variations, but we can obtain a simplified problem by parameterizing the variational model q [12]. First, we assume it factorizes according to:

$$q(x_k, \Sigma_k, \xi_k, \lambda_k) = q_x(x_k) q_\Sigma(\Sigma_k) q_\xi(\xi_k) q_\lambda(\lambda_k). \quad (14)$$

Then, we impose the following parametric distributions:

$$q_x(x_k) \triangleq \mathcal{N}(x_k | m_k, S_k) \quad (15a)$$

$$q_\Sigma(\Sigma_k) \triangleq \mathcal{IW}(\Sigma_k | \Lambda_k, \nu_k) \quad (15b)$$

$$q_\xi(\xi_k) \triangleq \mathcal{G}(\xi_k | \alpha_k, \beta_k) \quad (15c)$$

$$q_\lambda(\lambda_k) \triangleq \mathcal{G}(\lambda_k | \gamma_k, \delta_k). \quad (15d)$$

The free energy functional is now an objective function with respect to $\phi = \{m_k, S_k, \Lambda_k, \nu_k, \alpha_k, \beta_k, \gamma_k, \delta_k\}$. The optimal form of each factor consists of a marginalization with respect to the other factors [11]. The optimal form of the state factor is:

$$\begin{aligned} q_x(x_k) &\propto \exp \left(\mathbb{E}_{q_\Sigma, q_\xi} \left[\log p(x_k, \Sigma_k, \xi_k | o_{1:k-1}) \right] \right. \\ &\quad \left. + \mathbb{E}_{q_\lambda} \left[\log p(o_k, \lambda_k | x_k) \right] \right), \end{aligned} \quad (16)$$

which - when solved - yields the following update equations for its parameters:

$$m_k = \mu_k |_{k-1} + K_k(o_k - H_k \mu_k |_{k-1}) \quad (17a)$$

$$S_k = \tilde{S}_k - K_k H_k \tilde{S}_k, \quad (17b)$$

with Kalman gain $K_k = \tilde{S}_k H_k^\top (H_k \tilde{S}_k H_k^\top + \tilde{R}_k)$. The auxiliary matrices \tilde{S}_k and \tilde{R}_k correspond to the expectations of the scaled covariance matrix of the prior predictive and the scaled covariance of the likelihood:

$$\tilde{S}_k = \frac{1}{\nu_k - D_x - 1} \Lambda_k \frac{\beta_k}{\alpha_k}, \quad \tilde{R}_k = R_k \frac{\delta_k}{\gamma_k}. \quad (18)$$

For a more detailed description of the derivations involved in, see [6]. Note that the covariance matrix S_k of the factor is now time-varying, as it depends on the current belief over the process noise covariance matrix Σ_k . Solving for the other factors is more straightforward as they only appear in term each. The inverse-Wishart distributed factor for Σ_k has the following optimal form:

$$q_\Sigma(\Sigma_k) \propto \exp(\mathbb{E}_{q_x, q_\xi}[\log p(x_k, \Sigma_k, \xi_k | o_{1:k-1})]), \quad (19)$$

which gives the parameter update equations:

$$\Lambda_k = U_k + \frac{\alpha_k}{\beta_k} C_x, \quad \nu_k = u_k + 1 \quad (20)$$

where $C_x = S_k + (m_k - \mu_k |_{k-1})(m_k - \mu_k |_{k-1})^\top$. The factor for the process scale parameter ξ_k has an optimal form of:

$$q_\xi(\xi_k) \propto \exp(\mathbb{E}_{q_\Sigma, q_x}[\log p(x_k, \Sigma_k, \xi_k | o_{1:k-1})]), \quad (21)$$

yielding parameter updates:

$$\alpha_k = \frac{1}{2}(D_x + s), \quad \beta_k = \frac{1}{2}(s + \text{tr}(C_x(\nu_k + D_x - 1)\Lambda_k^{-1})). \quad (22)$$

Finally, the factor for the measurement noise scale parameter λ_k is optimal when:

$$q_\lambda(\lambda_k) \propto \exp(\mathbb{E}_{q_x}[\log p(o_k, \lambda_k | x_k)]), \quad (23)$$

yielding parameter update equations:

$$\gamma_k = \frac{1}{2}(D_o + v), \quad \delta_k = \frac{1}{2}(v + \text{tr}(C_o R_k^{-1})), \quad (24)$$

where $C_o = (o_k - H m_k)(o_k - H m_k)^\top + H S_k H^\top$. These update equations are a form of exact coordinate descent on $\mathcal{F}_k[\phi]$ [11]. It typically takes less than 10 iterations to reach convergence.

C. Robust Gaussian Sum Filter Implementation

The desired robust sum filter is achieved simply by replacing the KF block with RSTKF block, which is responsible of calculating the conditional posterior distribution $p(x_k | Z_k, \theta_k)$. The resulting algorithm will be referred as *RSTKF-GSF*. Swapping the KF block affects the computation of the mixture weights since these require the calculation of $p(z_k^{\theta_k})$. However, that term becomes intractable. We approximate it using the formula for weight computation under the standard GSF.

Fig. 2 shows the performance of the *RSTKF-GSF* in the same scenario as Fig. 1. It is robust to the sudden large drop in velocity that caused the GSF to start drifting.

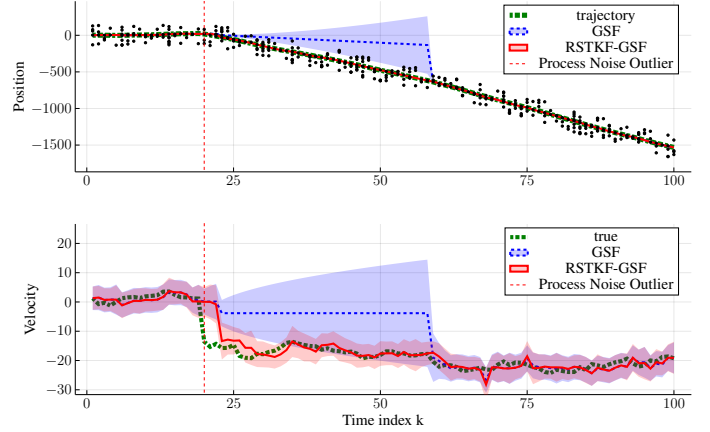


Fig. 2: Same simulation as in Fig. 1, including the estimates using *RSTKF-GSF*(red-solid). The performance of *RSTKF-GSF* does not degrade substantially after encountering the outlier process noise.

IV. EXPERIMENTS

In this section, we compare the performance of RSTKF-GSF with the original GSF algorithm on a simulated scenario for single object tracking in clutter. Four different Monte Carlo simulations were performed, where the process and the measurement noise are both Gaussian in the first scenario. The second scenario simulates heavy-tailed process noise and Gaussian measurement noise. The third scenario simulates Gaussian process noise and heavy-tailed measurement noise. The fourth scenario simulates both heavy-tailed process and measurement noise.

A. Simulation Setting

The simulation setting and performance metric is similar to given in [6]. Each Monte Carlo simulation consist of 100 time steps. The trajectory is simulated with a single target moving according to a constant velocity model in 2-D space and the position of the target is observed. The state at time step k is defined as $x_k \triangleq [p_{x,k}, p_{y,k}, v_{x,k}, v_{y,k}]^\top$, where $(p_{x,k}, p_{y,k})$ is the position of the target and $(v_{x,k}, v_{y,k})$ is the velocity of the target in Cartesian coordinates in x-axis and y-axis, respectively. The linear state space model is used given in (3). The parameters of the dynamics are set as follows:

$$F = \begin{bmatrix} I_2 & \Delta_t I_2 \\ \mathbf{0}_2 & I_2 \end{bmatrix}, \quad Q = \begin{bmatrix} \frac{\Delta_t^3}{3} I_2 & \frac{\Delta_t^2}{2} I_2 \\ \frac{\Delta_t^2}{2} I_2 & \Delta_t I_2 \end{bmatrix}, \quad (25)$$

where I_2 is the 2-D identity matrix, $\mathbf{0}_2$ is the 2×2 matrix of zeros, $\Delta_t = 1$ is the sampling rate. The parameters of the measurement process are:

$$H = [I_2 \quad \mathbf{0}_2], \quad R = r I_2, \quad (26)$$

where $r = 10$. The process model is simulated according to:

$$\omega_k \sim \begin{cases} \mathcal{N}(0, Q) & \text{w.p. } P_\omega \\ \mathcal{N}(0, 100Q) & \text{w.p. } 1 - P_\omega \end{cases}, \quad (27)$$

where "w.p." is shorthand for "with probability". The measurement model is simulated with:

$$v_k \sim \begin{cases} \mathcal{N}(0, R) & \text{w.p. } P_v \\ \mathcal{N}(0, 100R) & \text{w.p. } 1 - P_v \end{cases} \quad (28)$$

The set of parameters for each experiment case is summarized in Table. I. Chosen values of P_ω and P_v are used to simulate heavy-tailed noise [6].

TABLE I: P_ω and P_v parameters of experiments.

Exp. #	Process Noise	Measurement Noise	P_ω	P_v
1	Gaussian	Gaussian	1.00	1.00
2	Heavy-Tailed	Gaussian	0.95	1.00
3	Gaussian	Heavy-Tailed	1.00	0.90
4	Heavy-Tailed	Heavy-Tailed	0.95	0.90

Each experiment consist of $M = 1000$ Monte Carlo simulations comparing the Root Mean Square Errors (RMSE) at each time step, for both position and velocity.

The clutter is sampled from a Poisson Point Process with rate parameter 3. The spatial pdf is uniform around the true state position with a range of $\pm 15r$, i.e., 150. The probability of detection P_D was set to 0.95, which is the value used for both simulating the data and for both GSF filters. The clutter intensity function $\lambda_c(\cdot)$ is assumed to be constant and set to $3/(2 \cdot 15 \cdot r)^2$. Mixture reduction parameters are set as $\gamma_{prune} = 6.25 \cdot 10^{-6}$ and $N_{max} = 10$ for both filters. Weight calculations are also identical in order to compare filtering algorithms.

B. Results

In radar object tracking, cars will not always behave according to constant-velocity model and sudden brakes or accelerations cause outliers in the state transitions. This corresponds to the setting with heavy-tailed process noise and just Gaussian measurement noise. The simulation results of this scenario are shown in Fig. 3. They show that the *RSTKF-GSF* outperforms the GSF. This is expected since *RSTKF-GSF* models heavy-tailed noise characteristics whereas GSF assumes Gaussian process noise.

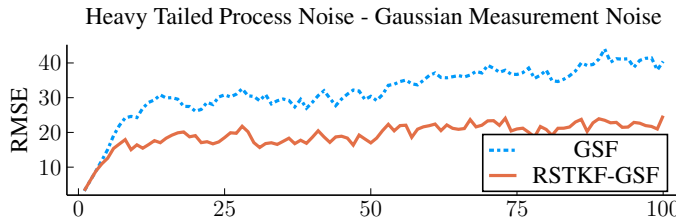


Fig. 3: Experiment-2 with heavy-tailed process noise and Gaussian distributed measurement noise. Root mean square errors over time of GSF (blue-dashed) versus RSTKF-GSF (red-solid).

Similarly, the *RSTKF-GSF* preserves its robustness compared to the GSF when both process and measurement noise are heavy-tailed. This result is shown in Fig. 4.

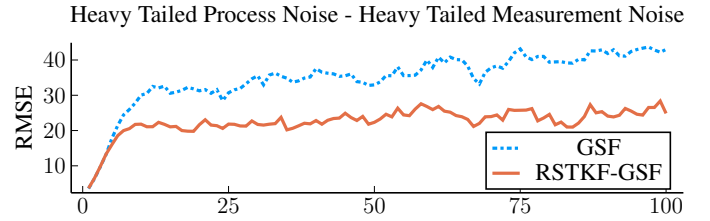


Fig. 4: Experiment-4 with heavy-tailed process noise and measurement noise. Root mean square errors over time of GSF (blue-dashed) versus RSTKF-GSF (red-solid).

Fig. 5 and Fig. 6 show that when the process noise is Gaussian, i.e., no outlier in the process, both filters perform similarly in terms of RMSE.

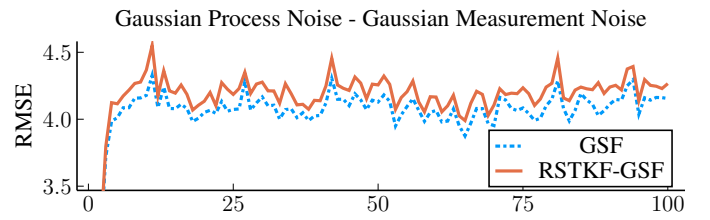


Fig. 5: Experiment-1 with Gaussian distributed process noise and measurement noise. Root mean square errors over time of GSF (blue-dashed) versus RSTKF-GSF (red-solid).

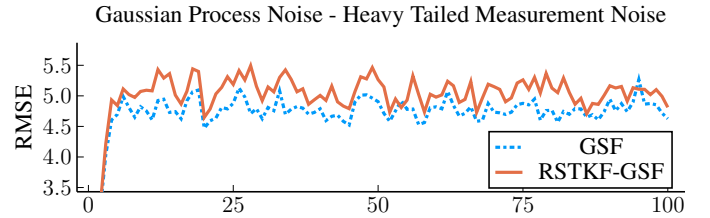


Fig. 6: Experiment-3 with Gaussian distributed process noise and heavy-tailed measurement noise. Root mean square errors over time of GSF (blue-dashed) versus RSTKF-GSF (red-solid).

C. Computational cost

The filtering parts of both algorithms are also compared in terms of computation time. The RSTKF performs several parameter updates in each time step to reach convergence. We obtain results in Sec. IV-B using 10 iterations per time step, but we observed that 5 iterations per time step were sufficient for posterior parameters to converge. Fig. 7 compares the median wall clock time of RSTKF function with varying number of iterations and the KF function. We observe that using the RSTKF algorithm with 10 iterations does not introduce considerable computational costs, and RSTKF is feasible to use in real-time applications.

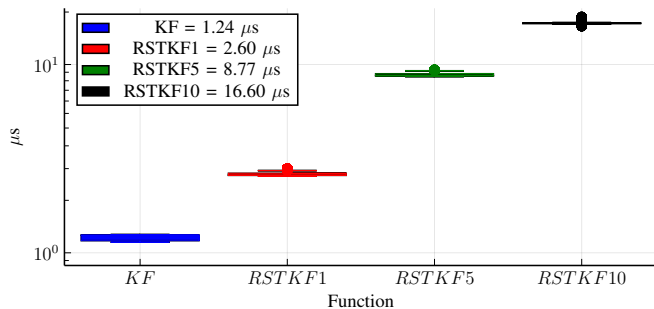


Fig. 7: Median wall clock time of KF (blue) versus RSTKF with 1 (red), 5 (green) and 10 (black) iterations. Results for the inner 90th percentile are shown on logarithmic scale.

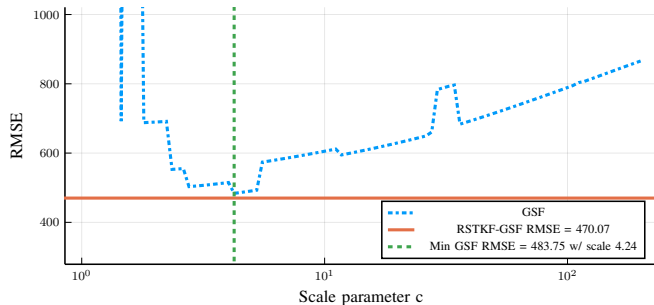


Fig. 8: Total root mean square errors vs. scale of process noise covariance Q . Vertical line (green) indicates the scale of Q for which the GSF estimate (blue) attains its minimum RMSE, which is still higher than the *RSTKF-GSF* estimate (red).

D. Adaptive estimation versus tuning

We compared our *RSTKF-GSF* with tuning the process noise covariance matrix Q of the GSF tracker on the same data as in Fig. 1 and Fig. 2. Manual tuning is performed by introducing a scale parameter c and using $\hat{Q} = c \cdot Q$ as our process covariance matrix. 100 points are sampled starting from 1 to 200 on a logarithmic scale to use as the scale parameter c . Fig. 8 shows the comparison of the total RMSE achieved as a function of the scale parameter of Q . It is observed that GSF could not beat *RSTKF-GSF* with a fixed process covariance matrix \hat{Q} .

V. DISCUSSION

Although there is no explicit modeling of heavy-tailed noise characteristics for process and measurement noise, the GSF is still robust to the heavy-tailed measurement noise (see Fig. 6). This implicit effect comes from the marginalisation of the data association variable θ_k . When the measurement is corrupted with heavy-tailed noise, the resulting value will be uninformative and will be viewed as clutter. If it's seen as clutter, then the object is misdetected. Thus, even though heavy-tailed measurement noise characteristics are not modeled explicitly, using a mixture representation and including the misdetection hypothesis introduces measurement outlier robustness to the GSF algorithm.

We also noted that the weight calculation involves calculating the evidence term $p(z_k^{\theta_k})$, which is intractable for

the *RSTKF-GSF* and is approximated. In addition, an outlier rejection method called gating can prevent the calculation of unlikely data association sequences by forming a gate around each hypothesis and rejecting all measurements outside it. The most typical form is ellipsoidal gating; it assumes additive Gaussian measurement noise and is invalid for the *RSTKF-GSF* case. Non-ellipsoidal gating can be used for such methods, but that is also based on a lower bound approximation of the evidence term $p(z_k^{\theta_k})$. For more details about non-ellipsoidal outlier rejection and the lower bound of the evidence under heavy-tailed measurement noise, we refer the interested reader to [13].

VI. CONCLUSION

We presented an extension of the Gaussian Sum Filter, a state-of-the-art method for single object tracking using radar. Instead of a Gaussian noise model, we adopted a heavy-tailed Student's t-distribution, which accounts for the system undergoing sudden state changes. We demonstrated that our algorithm, the *RSTKF-GSF*, is robust to these process outliers and does not lose track as easily. Furthermore, our simulations showed that the algorithm performs equivalently to the GSF when process outliers were absent and only presents a modest increase in computational cost.

REFERENCES

- [1] J. Vargas, S. Alsweiss, O. Toker, R. Razdan, and J. Santos, "An Overview of Autonomous Vehicles Sensors and Their Vulnerability to Weather Conditions," *Sensors (Basel, Switzerland)*, vol. 21, Aug. 2021.
- [2] A. Manjunath, Y. Liu, B. Henriques, and A. Engstle, "Radar Based Object Detection and Tracking for Autonomous Driving," in *IEEE MTT-S International Conference on Microwaves for Intelligent Mobility*, pp. 1–4, Apr. 2018.
- [3] Y. Bar-Shalom and X.-R. Li, *Multitarget-Multisensor Tracking: Principles and Techniques*. Storrs, Conn: YBS, 3rd printing ed., 1995.
- [4] H. Masnadi-Shirazi, A. Masnadi-Shirazi, and M.-A. Dastgheib, "A Step by Step Mathematical Derivation and Tutorial on Kalman Filters," *arXiv:1910.03558 [stat]*, Oct. 2019.
- [5] Y. Ho and R. Lee, "A Bayesian Approach to Problems in Stochastic Estimation and Control," *IEEE Transactions on Automatic Control*, vol. 9, pp. 333–339, Oct. 1964.
- [6] Y. Huang, Y. Zhang, N. Li, Z. Wu, and J. A. Chambers, "A Novel Robust Student's t-Based Kalman Filter," *IEEE Transactions on Aerospace and Electronic Systems*, vol. 53, pp. 1545–1554, June 2017.
- [7] S. Särkkä, *Bayesian Filtering and Smoothing*. London ; New York: Cambridge University Press, Oct. 2013.
- [8] B.-T. Vo, B.-N. Vo, and A. Cantoni, "Bayesian Filtering with Random Finite Set Observations," *IEEE Transactions on Signal Processing*, vol. 56, pp. 1313–1326, Apr. 2008.
- [9] A. Runnalls, "Kullback-Leibler Approach to Gaussian Mixture Reduction," *IEEE Transactions on Aerospace and Electronic Systems*, vol. 43, pp. 989–999, July 2007.
- [10] Y. Huang, Y. Zhang, P. Shi, Z. Wu, J. Qian, and J. A. Chambers, "Robust Kalman Filters Based on Gaussian Scale Mixture Distributions with Application to Target Tracking," *IEEE Transactions on Systems, Man, and Cybernetics: Systems*, vol. 49, pp. 2082–2096, Oct. 2019.
- [11] D. M. Blei, A. Kucukelbir, and J. D. McAuliffe, "Variational Inference: A Review for Statisticians," *Journal of the American Statistical Association*, vol. 112, pp. 859–877, Apr. 2017. arXiv: 1601.00670.
- [12] S. Sarkka and A. Nummenmaa, "Recursive noise adaptive Kalman filtering by variational Bayesian approximations," *IEEE Transactions on Automatic control*, vol. 54, no. 3, pp. 596–600, 2009.
- [13] G. Agamennoni, J. I. Nieto, and E. M. Nebot, "Approximate Inference in State-Space Models with Heavy-Tailed Noise," *IEEE Transactions on Signal Processing*, vol. 60, pp. 5024–5037, Oct. 2012.